IEEE Open Journal of
Antennas and Propagation

Received 29 November 2020; revised 28 December 2020; accepted 3 January 2021. Date of publication 13 January 2021; date of current version 8 February 2021.

Digital Object Identifier 10.1109/OJAP.2021.3051478

Embedded Propagation Graph Model for Reflection and Scattering and Its Millimeter-Wave Measurement-Based Evaluation

YUAN LIU [1,2], XUEFENG YIN [1,3] (Member, IEEE), XIAOKANG YE [1] (Student Member, IEEE), YONGYU HE [1] (Student Member, IEEE), AND JUYUL LEE [4] (Senior Member, IEEE)

[1]College of Electronics and Information Engineering, Tongji University, Shanghai 200092, China

[2]Guangdong Communications & Networks Institute, Guangzhou, China

[3]National Computer and Information Technology Practical Education Demonstration Center, Tongji University, Shanghai 200092, China

[4]Telecommunication and Media Research Laboratory, Electronics and Telecommunications Research Institute, Daejeon 34129, South Korea

CORRESPONDING AUTHOR: X. YIN (e-mail: yinxuefeng@tongji.edu.cn)

This work was supported in part by the China National Science Foundation General Project under Grant 61971313, and in part by the Institute for Information & Communications Technology Planning & Evaluation (IITP) grant funded by the Korean Government (MSIT, Development of Time-Space Based Spectrum Engineering Technologies for the Preemptive Using of Frequency).

ABSTRACT Propagation graph (PG) is a stochastic channel simulation method for scattering propagation. In this article, an embedded-PG (EPG) approach, an extension of conventional PG, is proposed to simulate reflection and scattering multi-path behaviors in wireless channels. In this method, multiple propagation paths are categorized into scattering-path, reflecting-path, and scattering-reflecting mixed paths among reflectors and scatterers. The matrix recursive formula of conventional PG modeling is used to calculate scattering-path, a recursive mathematical transformation is applied to adapt reflecting-path into the recursive formula, and an embedded graph method is used to decompose mixed-path into scattering effects and reflection effects. The proposed simulation approach is validated by comparison with conventional PG and measurement in 39 GHz millimeter-wave (mm-wave) time-variant corridor scenario. Power delay profiles (PDPs) and spatial consistency of multiple paths observed in concatenated-PDPs (CPDPs) obtained by EPG are more consistent with measurement than conventional PG, differences of mean delay and delay spread between simulations and measurement in typical snapshots are within 3 ns and 1.5 ns, respectively.

INDEX TERMS Channel modeling, channel simulation, millimeter-wave channel, reflection-embedded propagation graph, time-variant channel.

I. INTRODUCTION

DESIGN of algorithm and performance optimization for next generation of wireless communication systems become research focus both in the academia and industry, owing to the rapid increase in the need of channel bandwidth and data rate [1]–[3]. Channel modeling of millimeter-wave (mm-wave) is essential for 5G and beyond wireless communication systems [4]. There are two typical approaches to characterizing parameters of channel modeling, i.e., measurement-based and simulation-based [5]. However, measurement-based channel models concentrate on statistical behaviors, which require abundant experimental data [6]. Meanwhile, challenges in carrying out field measurements increase drastically in mm-wave bands, so as the deployment costs. As a result, an accurate and efficient simulation-based method is of great necessity for mm-wave and higher-frequency band channels.

Geometry-based channel simulation tools have a significant advantage on predicting the specific propagating path in space and spatial information over other simulation methods, e.g., room electro-magnetics. With those information, it is possible to study the the spatial consistency and space-time randomness of channels, multi-path clustering and so on. The most widely used geometry-based channel simulation

TABLE 1. Summary of state-of-the-art geometry-based channel simulation algorithms.

Algorithms	Methods and applications	Features and comments
Ray tracing (RT)	Deterministic simulation algorithm, which mainly makes use of image method to calculate geometrical optic rays and has been widely used [7], [8], [11], [12]	Advantages: (1) is able to calculate reflection, scattering, and diffraction mechanisms [13]–[15]; (2) good simulation accuracy; shorts: (1) high time consumption; (2) hard to include reverberating effects among different propagation mechanisms
Propagation graph (PG)	Stochastic simulation algorithm, which evaluates scattering effects by calculating scattering matrices [9], [10], [17], [18]; applications including: indoor room reverberating effects [19], [20], human blockage and doppler frequency UWB channel [21], high speed train channel [22], channel capacity of MIMO systems [25]	Advantages: (1) is able to reproduce the exponential power decay caused by high older bouncing; (2) absolute good time consumption over RT [30]; shorts: do not calculate reflection and diffraction propagation mechanisms
Hybrid modeling	Semi-deterministic simulation algorithm based on the combination of RT and PG, usually using RT to calculate reflection components and using PG to calculate scattering components [23], [30]–[32].	The scattering coefficients used in different models may vary; the time consumption is in between PG and RT
Modified PG	An iterative transfer matrix computation method for acceleration in room to room channel prediction [24]; a unified PG to approximately calculate specular reflection components [18]; an implementation of PG for multiple-knife-outdoor-diffraction scenario [26]; usage of machine learning to calibrate the scattering coefficients of PG [33]	All the modifications try to extend the usage of PG, at the same time keep the advantages on time consumption

methods are Ray-tracing (RT) [7], [8] and Propagation-graph (PG) model proposed in a recent decade [9], [10]. RT is a deterministic simulation tool, which makes use of image method to calculate geometrical optic rays of waves propagate along paths involving reflection [11], [12]. It is worthy mentioning that some commercial softwares of RT also include other basic propagation mechanisms, such as scattering and diffraction [13]–[15]. However, the shortages of RT are: (1) there is a high time and resource consumption for high order reflection calculations; (2) it is hard to include reverberating effects of different propagation mechanisms.

The PG is a stochastic simulation method, which mainly makes use of the topology structure of directed graph [16] to calculate the effect of wave propagation along paths involving scattering in matrices with a significant advantage in the reduction of computational compexity [17], [18]. For this reason, the PG model has been widely applied in channel simulations of variant scenarios after being originally proposed. For indoor and outdoor scenarios, the PG theory was used to predict closed room reverberating effects and exponential power decay [19], [20], human blockage and doppler frequency of ultra wide band (UWB) channel [21], and high speed train channels [22]. For multi-room channel predictions, PG and Rays were combined in [23], and an iterative transfer matrix computation method was used for acceleration in [24]. Furthermore, PG even showed interesting results in analyzing characteristics and channel capacity of Multiple-input-multiple-output (MIMO) systems [25].

Due to the efficiency and flexibility of PG, researchers contributed themselves to modifying the model by including reflection [18] and diffraction effects [26], which are also considered as the three basic propagation mechanisms along with scattering [27]–[29]. The most commonly used method is hybrid model, which combines PG and RT [30]–[32]. The main difference of [30], [31], and [32] is the calculation of scattering coefficients. Time efficiency of these two simulation algorithms were studied and compared in [30], which revealed that time consumption of PG grows linearly as bouncing order of wave increases, while that of RT grows exponentially, hence PG model owns obviously better performance on time consumption than RT when the reflection order is larger than three. A Summary of literature review is listed in Table 1.

To overcome the shortages of conventional PG mentioned in Table 1, a so-called embedded propagation graph (EPG) is proposed that can be used to predict wireless propagation channels with the capability of calculating both reflecting and scattering components. It may provide powerful tools for channel researches, e.g., multi-path clustering analysis in wireless channel, high frequency channel predictions, and other applications like radio based localizations.

Since EPG is an extension of conventional PG model, on the one hand, it inherits good time consumption of matrices calculation from PG; on the other hand, the accuracy is improved by considering reflection effects and reverberating effects of scattering and reflection. The technical novelties of the proposed algorithm can be concluded as:

1) Use PG model to calculate reflection effects in radio channel by applying a linear mathematic transformation to adapt the multi-bounce reflection into the recursive matrices formula.

2) Use embedded PG model to compute the reverberating paths between reflection and scattering by exploiting an embedded method to decompose the reverberating paths into scattering-path and reflecting-path.

3) Evaluate the newly proposed EPG in a time-varying scenario using mm-wave frequency band.

The remaining parts of this article are arranged as follows: Section II introduces the methodology of EPG. Section III

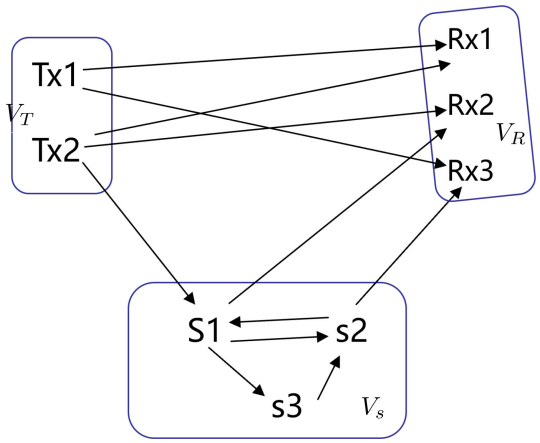

FIGURE 1. Vertices illustration for conventional PG model.

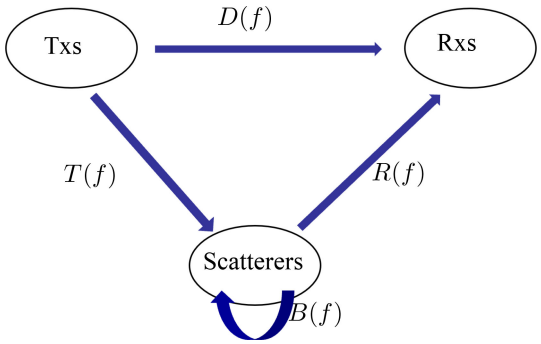

FIGURE 2. Transfer matrices model for conventional PG computation.

describes the procedure of EPG. The simulation results of EPG and its validation. Finally, conclusive remarks are given in Section IV.

II. METHODOLOGY

A. REVISIT OF SCATTERING PROPAGATION GRAPH THEORY AND ITS MODIFICATION

A wireless communication system generally contains transmitters (Txs), receivers (Rxs), and environment that wave propagating through. The conventional PG proposed in [19], [20] is based on the assumption that the environment is discretized as scattering points. Scattering points, Txs, and Rxs are regarded as vertices V_s, V_T, and V_R in a propagation graph, respectively, as Fig. 1 shows. The paths among these vertices are defined as edges ε_d, ε_{Ts}, ε_{Rs}, and ε_{ss}, which represent edges of V_T to V_R, V_T to V_s, V_s to V_R, and V_s to V_s, respectively.

The transfer coefficient of a propagation edge connecting two vertices in the graph can be expressed as

$$A_{\mathrm{e}}(f) = \mid g_{\mathrm{e}}(f) \mid \cdot \exp(-j2\pi f\tau_e + j\phi), \tag{1}$$

where f is the carrier frequency of signal, ϕ can be regarded as a random variable following uniform distribution on the interval $[0,\ 2\pi)$, $|g_{\mathrm{e}}(f)|$ is the edge gain, which can be defined as

$$|g_{\mathrm{e}}(f)|^2 = \begin{cases} \left(\dfrac{c}{4\pi\tau_e f}\right)^2, & \mathrm{e} \in \varepsilon_d \\ \dfrac{1}{4\pi f \mu_{(\varepsilon_{Ts})}} \cdot \dfrac{\tau_e^{-2}}{S(\varepsilon_{Ts})}, & \mathrm{e} \in \varepsilon_{Ts} \\ \dfrac{1}{4\pi f \mu_{(\varepsilon_{Rs})}} \cdot \dfrac{\tau_e^{-2}}{S(\varepsilon_{Rs})}, & \mathrm{e} \in \varepsilon_{Rs} \\ \dfrac{g^2}{odi(e)^2}, & \mathrm{e} \in \varepsilon_{ss} \end{cases} \tag{2}$$

where $odi(e)$ denotes the out degree of the corresponding scatterers, and for any edges belong to ε

$$\mu(\varepsilon) = \frac{1}{|\varepsilon|}\sum_{e=\varepsilon}\tau_e \text{ and } \mathrm{S}(\varepsilon) = \sum_{e\in\varepsilon}\tau_e{}^{-2}, \tag{3}$$

in which

$$\tau_{\mathrm{e}} = \frac{d_e}{c} \text{ with } \mathrm{d_e} = |\boldsymbol{r}_v - \boldsymbol{r}_{v'}|, \tag{4}$$

where c is the speed of light, $|.|$ denotes two dimensional norm, $\boldsymbol{r}_v$ and $\boldsymbol{r}_{v'}$ denote position vectors of vertices of any edges.

Then, define $\boldsymbol{D}(f)$, $\boldsymbol{T}(f)$, $\boldsymbol{R}(f)$, and $\boldsymbol{B}(f)$ denote the transfer matrices from vertices V_T to V_R, from V_T to V_s, from V_s to V_R, and from V_s to V_s, respectively, the transfer matrices model is illustrated by Fig. 2. The channel transfer function can be calculated as [20]

$$\begin{aligned} \boldsymbol{H}(f) &= \boldsymbol{D}(f) + \boldsymbol{R}(f)\left[\boldsymbol{I} + \boldsymbol{B}(f) + \cdots + \boldsymbol{B}^n(f)\right]\boldsymbol{T}(f) \\ &= \boldsymbol{D}(f) + \boldsymbol{R}(f)\left[\boldsymbol{I} - \boldsymbol{B}(f)\right]^{-1}\boldsymbol{T}(f), \end{aligned} \tag{5}$$

where I is identity matrix. The PG model can evaluate the effects of infinite-bounce among scatterers by calculating a matrix inverse.

The term $odi(e)$ in Eq. (2) ensures that the total outbounding power does not exceed the input power, however, it also results in the transmitting power is uniformly distributed to other scatterers. For this reason, a semi-deterministic approach is proposed to modify the edge gain in [30], [31] as

$$|g_{\mathrm{e}}(f)|^2 = \begin{cases} \left(\dfrac{c}{4\pi d_e f}\right)^2, & \mathrm{e} \in \varepsilon_d \\ \dfrac{\mathrm{d}S \cdot \cos(\theta_i)}{4\pi d_e^2}, & \mathrm{e} \in \varepsilon_{Ts} \\ \dfrac{S^2 \cdot \cos(\theta_s)}{\pi d_e^2} \cdot \dfrac{c^2}{4\pi f^2}, & \mathrm{e} \in \varepsilon_{Rs} \\ \dfrac{S^2 \cdot \mathrm{d}S \cdot \cos(\theta_{i2})\cos(\theta_{s1})}{\pi d_e^2}, & \mathrm{e} \in \varepsilon_{ss} \end{cases} \tag{6}$$

where S represents the scattering loss, dS denotes the area of the small tile at scatterers, θ_i represents the angle between incident direction of a wave and the normal vector of a scattering surface, θ_s represents the angle between scattering direction of a wave and the normal vector of a scattering surface. It is verified by measurement that the modified edges gains obtain a better accuracy than conventional PG model. Thus, the modified edge gains is applied for the proposed EPG in this article.

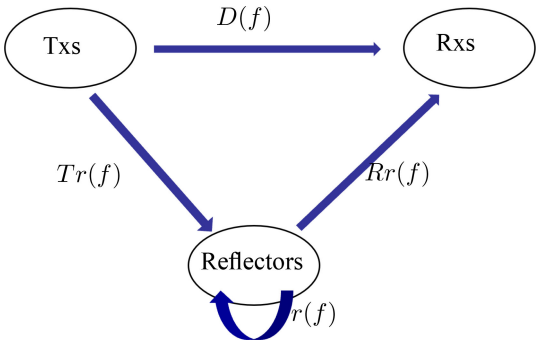

FIGURE 3. Transfer matrices model for EPG computation.

B. CALCULATION OF REFLECTION PROPAGATION GRAPH

Define a new Reflection Propagation Graph (RPG) which contains only Txs, Rxs and reflectors. To discretize them into vertices as V_T, V_R and V_r, then the transfer matrices model can be illustrated as Fig. 3. The paths among these vertices are defined as ε_d, ε_{Tr}, ε_{Rr} and ε_{rr}, which represent edges from V_T to V_R, V_T to V_r, V_r to V_R, and V_r to V_r, respectively.

The Line-of-sight (LoS) paths of RPG can be calculated as the same method of PG. For simplification, only introduce Non-LoS (NLoS) paths in the following discussion.

1) ANALYSIS OF EDGE GAINS FOR REFLECTION AND SCATTERING

For multiple scattering propagation, the edge gain contains a product of distances multiplication. For example, the Friis equation in [34] describes received power gain after bouncing sequentially with n scatterers named No. $1, 2, \ldots, (n+1)$, i.e., the radio wave propagating through n edges can be calculated as

$$P_{\mathrm{n}+1} = P_1 \cdot S^n \cdot \left(\frac{\lambda}{4\pi\,(d_1 \cdot d_2 \cdot \cdots \cdot d_n)}\right)^2, \tag{7}$$

where $P_{\mathrm{n}+1}$ represents the received power, P_1 is the transmitted power, d_n denotes the distance between the NO.n to the NO.$(n+1)$ scatterer. Thus, the scattering matrices $\boldsymbol{B}(f)^n$ can be used to calculate the overall transfer matrix of signal scattering n times among the scatterers.

However, for reflection, the received power after reflecting through $(n+1)$ reflectors contains a factor of distances addition [34], i.e., radio wave propagating through n edges can be calculated as

$$P_{\mathrm{n}+1} = P_1 \cdot R^n \left(\frac{\lambda}{4\pi\,(d_1 + d_2 + \cdots + d_n)}\right)^2, \tag{8}$$

where R is polarimetric reflection loss [35]. Equation (8) shows that the power gain for multiple-reflection is dependent on the additive distances of all the paths. Since distance-factor can not be multiplied sequentially, the continuous matrices multiplication of PG are hard to be directly used for calculating the effect of n-bounce reflection. To adapt the reflection in the framework of conventional PG iterative matrices operation, we have to calculate distance factors separately.

2) FACTORIZATION OF EDGE GAINS OF RPG

The propagation gain for any edges can be factorized into gain-factor and distance-factor, i.e.,

$$|g_{\mathrm{e}}(f)|^2 = \left|g_{\mathrm{gain}}(f)\right|^2 \cdot \left|g_{\mathrm{path}}\right|^2, \tag{9}$$

where gain-factor $g_{gain}(f)$ can be calculated based on Eq. (6) as

$$\left|g_{\mathrm{gain}}(f)\right|^2 = \begin{cases} \dfrac{\mathrm{d}S \cdot \cos(\theta_i)}{4\pi}, & \mathrm{e} \in \varepsilon_{Tr} \\ \dfrac{S^2 \cdot \cos(\theta_s)}{\pi} \cdot \dfrac{c^2}{4\pi f^2}, & \mathrm{e} \in \varepsilon_{Rr} \\ \dfrac{S^2 \cdot \mathrm{d}S \cdot \cos(\theta_{i2})\cos(\theta_{s1})}{\pi}, & \mathrm{e} \in \varepsilon_{rr} \end{cases} \tag{10}$$

and g_{path} contains the edge distance-factor, we proposed a recursive mathematical transformation to calculate it.

3) A MATHEMATICAL TRANSFORMATION FOR *N*-BOUNCE REFLECTION

Continuous addition of distance D_n is defined as

$$\begin{cases} D_{\mathrm{n}} = \frac{1}{d_1+d_2+\cdots+d_n}, & n \geq 2 \\ D_1 = \frac{1}{d_1}, & n = 1 \end{cases} \tag{11}$$

Applying the following manipulation, we can obtain a sequential approach for calculating D_n based on D_{n-1} as:

$$\begin{aligned} D_{\mathrm{n}} &= \frac{1}{d_1 + d_2 + \cdots + d_{n-1}} \cdot \frac{1}{1 + \frac{d_n}{d_1+d_2+\cdots+d_{n-1}}} \\ &= D_{\mathrm{n}-1} \cdot \frac{1}{1 + D_{\mathrm{n}-1} d_n} \\ &= D_{\mathrm{n}-1} \cdot \frac{1}{d'_n} \end{aligned} \tag{12}$$

with d'_n defined as the so-called equivalent distance

$$d'_{\mathrm{n}} \triangleq 1 + D_{\mathrm{n}-1} \cdot d_{\mathrm{n}}, n \geq 2. \tag{13}$$

Then using the mathematical transformation of Eq. (11), once the distances between vertices in the propagation graph are determined, the new distance d'_n can be calculated sequentially by $D_{\mathrm{n}-1}$ and d_n.

4) CALCULATION OF DISTANCE-FACTOR G_{PATH} OF RPG

(1) For one-bounce reflection, the propagation paths are: $Tx \rightarrow reflectors \rightarrow Rx$. The distances of Tx to reflectors, as well as reflectors to Rx are known. Use $\boldsymbol{d_{Tr}}$ to denote the distance matrix of Tx and reflectors, and $\boldsymbol{d_{Rr}}$ to denote the distance matrix of Rx and reflectors. Apply (11) and (13), we obtain

$$\begin{cases} \boldsymbol{D_1} = \frac{\boldsymbol{I}}{\boldsymbol{d_{Tr}}}, \\ \boldsymbol{d'_2} = \boldsymbol{I} + \boldsymbol{D_1} \cdot \boldsymbol{d_{Rr}}. \end{cases} \tag{14}$$

Then g_{path} can be calculated as

$$\left|g_{\text{path}}\right| = \begin{cases} \boldsymbol{D_1}, & \text{e} \in \varepsilon_{Tr} \\ \dfrac{\boldsymbol{I}}{\boldsymbol{d'_2}}. & \text{e} \in \varepsilon_{Rr} \end{cases} \tag{15}$$

(2) For multiple reflection, the number of the propagation edges $n \geq 3$. Tx and Rx are at two terminals, and the propagated waves would interact with reflectors for $(n-1)$ times. Use distance matrix $\boldsymbol{d_{rr}}$ to denote distances among reflectors. We adapt $\boldsymbol{d_{rr,i}}$ to denote the distance of the ith to the $(i+1)$th reflecting paths, $i \in [1, n-2]$. Hence the edge distance $\boldsymbol{d_2} \cdot \cdots \cdot \boldsymbol{d_{n-1}}$ are sequentially equal to the distance among reflectors $\boldsymbol{d_{rr,1}}$, $\boldsymbol{d_{rr,1}} \cdots \boldsymbol{d_{rr,(n-2)}}$, respectively. Apply the transformation (11) and (13), the n-time reflection can be represented as

$$\begin{cases} \boldsymbol{D_1} = \frac{\boldsymbol{I}}{\boldsymbol{d_{Tr}}}, \\ \cdots \\ \boldsymbol{d'_{n-1}} = \boldsymbol{I} + \boldsymbol{D_{n-2}} \cdot \boldsymbol{d_{n-1}} = \boldsymbol{I} + \boldsymbol{D_{n-2}} \cdot \boldsymbol{d_{rr,(n-2)}}, \\ \boldsymbol{D_{n-1}} = \boldsymbol{D_{n-2}} \cdot \dfrac{\boldsymbol{I}}{\boldsymbol{d'_{n-1}}}, \\ \boldsymbol{d'_n} = \boldsymbol{I} + \boldsymbol{D_{n-1}} \cdot \boldsymbol{d_n} = \boldsymbol{I} + \boldsymbol{D_{n-1}} \cdot \boldsymbol{d_{Rr}}. \end{cases} \tag{16}$$

Then, g_{path} can be calculated as

$$\left|g_{\text{path}}\right| = \begin{cases} \dfrac{\boldsymbol{I}}{\boldsymbol{d'_n}}. & \text{e} \in \varepsilon_{Rr} \\ \boldsymbol{D_1}, & \text{e} \in \varepsilon_{Tr} \\ \dfrac{\boldsymbol{I}}{\boldsymbol{d'_{n-1}}}. & \text{e} \in \varepsilon_{rr} \end{cases} \tag{17}$$

5) CALCULATION OF TRANSFER MATRICES AND CHANNEL TRANSFER FUNCTION OF RPG

We use $\boldsymbol{D}(f) \in \mathbb{C}^{1\times 1}$, $\boldsymbol{Tr}(f) \in \mathbb{C}^{1\times N}$, $\boldsymbol{Rr}(f) \in \mathbb{C}^{N\times 1}$ and $\boldsymbol{r}(f) \in \mathbb{C}^{N\times N}$ to denote the transfer matrices between the vertices V_T and V_R, V_T and V_r, V_r and V_R, V_r and V_r, respectively. Moreover, $\boldsymbol{Rr_n}(f) \in \mathbb{C}^{N\times 1}$ is introduced to denote the transfer matrix of reflectors to Rx after bouncing among reflectors for n times, $\boldsymbol{r_n}(f) \in \mathbb{C}^{N\times N}$ to denote the transfer function among reflectors after bouncing n times. Notice that $\boldsymbol{r_n}(f)$ is calculated sequentially based on the distance factor d'_{n-1} in Eq. (17).

For the transfer matrix, we also consider it in two parts as shown in (9), i.e., gain-factor and distance-factor.

Use $\boldsymbol{Tr_{gain}}(f)$ to denote the gain-factor transfer matrix of $\boldsymbol{Tr}(f)$, $\boldsymbol{Tr_{dis}}$ to denote the distance-factor transfer matrix of $\boldsymbol{Tr}(f)$, then $\boldsymbol{Tr}(f)$ can be calculated as

$$\boldsymbol{Tr}(f) = \boldsymbol{Tr_{gain}}(f) \odot \boldsymbol{Tr_{dis}}, \tag{18}$$

where $\odot$ means Hadamard product of matrices, $\boldsymbol{Tr_{gain}}(f)$ can be generated as (10), $\boldsymbol{Tr_{dis}}$ can be generated as (15) and (17).

Similarly, we use $\boldsymbol{r_{gain,n}}(f)$ to denote the gain-factor transfer matrix of $\boldsymbol{r_n}(f)$, $\boldsymbol{r_{dis,n}}$ to denote the distance-factor transfer matrix of $\boldsymbol{r_n}(f)$, then $\boldsymbol{r_n}(f)$ can be represented as

$$\boldsymbol{r_n}(f) = \boldsymbol{r_{gain,n}}(f) \odot \boldsymbol{r_{dis,n}}. \tag{19}$$

Algorithm 1 Modeling Algorithm of Pure Reflection Propagation Graph

Input: Geometrical information of scenario, electromagnetic properties of major reflecting materials, radiation pattern of antennas.

Output: Channel transfer function $\boldsymbol{H_{RPG}}(f)$.

Step 1: Divide surfaces into uniform small vertices, and obtain locations of reflecting vertices, Txs and Rxs.

Step 2: Generate distance matrices $\boldsymbol{d_{Tr}}$, $\boldsymbol{d_{Rr}}$, and $\boldsymbol{d_{rr}}$ based on locations in **Step 1**. Identify reflection paths based on snell' law. Then, calculate the iterative distance matrices $\boldsymbol{D_{rr,n}}$ and $\boldsymbol{d_{rr,n}}$.

Step 3: Generate gain-factor matrices $\boldsymbol{Tr_{gain}}(f)$, $\boldsymbol{r_{gain,n}}(f)$, and $\boldsymbol{Rr_{gain,n}}(f)$.

Step 4: Generate distance-factor matrices $\boldsymbol{Tr_{dis}}(f)$, $\boldsymbol{r_{dis,n}}(f)$, and $\boldsymbol{Rr_{dis,n}}(f)$.

Step 5: Calculate transfer matrices $\boldsymbol{Tr}(f)$, $\boldsymbol{r_n}(f)$, and $\boldsymbol{Rr_n}(f)$. Obtain channel transfer function $\boldsymbol{H_{RPG}}(f)$.

The first part $\boldsymbol{r_{gain,n}}(f)$ can be obtained as

$$\begin{aligned} \boldsymbol{r_{gain,n}}(f) &= \boldsymbol{r_{gain,(n-1)}}(f)\boldsymbol{r_{gain}}(f) \\ &= \boldsymbol{r_{gain}}^n(f), \end{aligned} \tag{20}$$

where entries in $\boldsymbol{r_{gain}}(f)$ can be generated as (10).

Use $\boldsymbol{Rr_{gain}, n}(f)$ to denote the gain-factor transfer matrix of $\boldsymbol{Rr_n}(f)$, and $\boldsymbol{Rr_{dis,n}}$ to denote the distance-factor transfer matrix of $\boldsymbol{Rr_n}(f)$. Thus, $\boldsymbol{Rr_n}(f)$ can be represented as

$$\boldsymbol{Rr_n}(f) = \boldsymbol{Rr_{gain,n}}(f) \odot \boldsymbol{Rr_{dis,n}}, \tag{21}$$

where the entries in $\boldsymbol{Rr_{gain}}(f)$ can be generated as Eq. (10), $\boldsymbol{Rr_{dis}}$ can be generated based on $\boldsymbol{d_{rr,n-1}}$ according to Eq. (17) and Eq. (24).

Finally, the NLoS part channel transfer function of RPG can be obtained as

$$\boldsymbol{H_{RPG}}(f) = \boldsymbol{Tr}(f)\boldsymbol{Rr_1}(f) + \sum_{n=2}^{\infty}\left[\boldsymbol{Tr}(f)\boldsymbol{r}_{n-1}(f)\boldsymbol{Rr_n}(f)\right]. \tag{22}$$

The implementation of RPG model can be summarized as the following flowchart.

In ***Step2***, to generate the distance-factor matrices $\boldsymbol{r_{dis,n}}$, it is necessary to consider the following aspects:

1) The $\boldsymbol{r_{dis,n}}$ is a sequentially result of the initial input $\boldsymbol{Tr_{dis}}$, $\boldsymbol{r_{dis,1}}$, $\boldsymbol{r_{dis,2}}$,..., and $\boldsymbol{r_{dis,n-1}}$.

2) Define $\boldsymbol{D_{rr,n}} \in \mathbb{C}^{N\times N}$ to denote the intermediate variable in (14) and (16).

3) Use matrix $\boldsymbol{C_{rr}}\mathbb{C}^{N\times N}$ to filter out the extra 1 elements resulted from term $(\boldsymbol{I} + \boldsymbol{D_{n-1}})$ in Eq. (16).

$\boldsymbol{C_{rr}}$ describes the relationship of every two reflectors, in which 1 means existing reflection path between the two reflectors and otherwise not. Define $\boldsymbol{d} \in \mathbb{C}^{N\times N}$ to denote the Euclidean space distance of every two reflectors, which can be obtained from digital map. So that the distance matrix of reflectors with connectivity $\boldsymbol{d_{rr}} \in \mathbb{C}^{N\times N}$ can be calculated as

$$\boldsymbol{d_{rr}} = \boldsymbol{d} \odot \boldsymbol{Check_{rr}}. \tag{23}$$

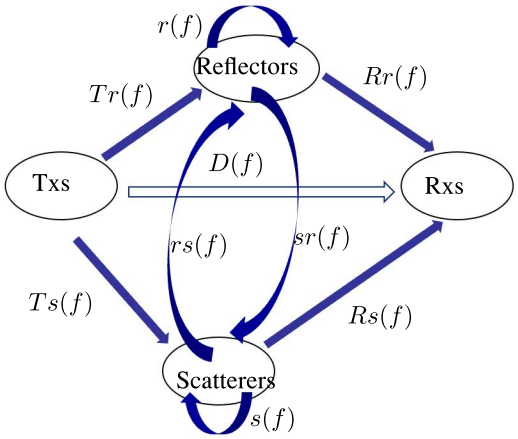

FIGURE 4. Diagram of PG with both Reflectors and Scatterers for Transfer function computation.

Apply the formulation of (16) on distances matrices $\boldsymbol{D_{rr,n}}$ and $\boldsymbol{d_{rr}}$, we obtain

$$\begin{cases} \boldsymbol{D_{rr,0}} = \left[\boldsymbol{Tr_{dis}}^T; \boldsymbol{Tr_{dis}}^T \cdots \boldsymbol{Tr_{dis}}^T\right], \\ \boldsymbol{d_{rr,1}} = \left(\boldsymbol{I} + \boldsymbol{D_{rr,0}} \odot \boldsymbol{d_{rr}}\right) \odot \boldsymbol{Check_{rr}}, \\ \cdots \\ \boldsymbol{d_{rr,n-1}} = \left(\boldsymbol{I} + \boldsymbol{D_{rr,n-2}} \cdot \boldsymbol{d_{rr}}\right) \odot \boldsymbol{Check_{rr}}^{n-1}, \\ \boldsymbol{D_{rr,n-1}} = \boldsymbol{D_{rr,n-2}} \cdot \dfrac{\boldsymbol{I}}{\boldsymbol{d_{rr,n-1}}}, \\ \boldsymbol{d_{rr,n}} = \left(\boldsymbol{I} + \boldsymbol{D_{rr,n-1}} \cdot \boldsymbol{d_{rr}}\right) \odot \boldsymbol{Check_{rr}}^{n}, \end{cases} \tag{24}$$

where $[.]^T$ denotes transpose of matrices.

Then $\boldsymbol{r_{dis,n}}$ can be calculated as

$$\boldsymbol{r_{dis,n}} = \frac{\boldsymbol{I}}{\boldsymbol{d_{rr,n}}}. \tag{25}$$

C. CALCULATION OF GRAPH WITH REFLECTORS AND SCATTERERS USING EPG

1) TRANSFER FUNCTION MODEL OF FULL PROPAGATION GRAPH

The EPG is expanded based on adding reflectors into the conventional scattering graph. Similarly to the conventional PG, we define the full propagation graph as shown in Fig. 4, which contains M1 transmitters, M2 receivers, N1 scatterers, and N2 reflectors. Then the transfer matrices can be defined as

$$\begin{aligned} \boldsymbol{D}(f) &\in \mathbb{C}^{M_1 \times M_2} : \text{transmitters} \rightarrow \text{receivers} \\ \boldsymbol{Ts}(f) &\in \mathbb{C}^{M_1 \times N_2} : \text{transmitters} \rightarrow \text{scatterers} \\ \boldsymbol{s}(f) &\in \mathbb{C}^{N_2 \times N_2} : \text{transmitters} \rightarrow \text{reflectors} \\ \boldsymbol{Rs}(f) &\in \mathbb{C}^{N_2 \times M_2} : \text{scatterers} \rightarrow \text{receivers} \\ \boldsymbol{Rr_n}(f) &\in \mathbb{C}^{N_1 \times M_2} : \text{reflectors} \rightarrow \text{receivers} \\ \boldsymbol{r}(f) &\in \mathbb{C}^{N_1 \times N_1} : \text{reflectors} \rightarrow \text{reflectors} \\ \boldsymbol{Tr}(f) &\in \mathbb{C}^{M_1 \times N_1} : \text{transmitters} \rightarrow \text{reflectors} \\ \boldsymbol{sr}(f) &\in \mathbb{C}^{N_2 \times N_1} : \text{reflectors} \rightarrow \text{scatterers} \\ \boldsymbol{rs}(f) &\in \mathbb{C}^{N_1 \times N_2} : \text{scatterers} \rightarrow \text{reflectors}. \end{aligned}$$

Matrices $\boldsymbol{D}(f)$, $\boldsymbol{Ts}(f)$, $\boldsymbol{s}(f)$ and $\boldsymbol{Rs}(f)$ can be calculated in similar manner as in Eq. (6). Matrices $\boldsymbol{Rr_n}(f)$, $\boldsymbol{r_n}(f)$ and $\boldsymbol{Tr}(f)$ can be calculated as using the RPG approach illustrated in Eq. (18), (19) and (21), respectively.

Matrix $\boldsymbol{sr}(f)$ and $\boldsymbol{rs}(f)$ contain the so-called mixed paths, which are reverberating bounces among reflectors and scatterers, i.e., the transfer matrix $\boldsymbol{sr}(f)$ contains the signal flows of the two components as

$$\begin{aligned} &case\ 1 : Tx \rightarrow reflectors \rightarrow scatterers, \\ &case\ 2 : Tx \rightarrow scatterers \rightarrow reflectors \rightarrow scatterers, \end{aligned}$$

and matrix $\boldsymbol{rs}(f)$ contains signal flows of two components as

$$\begin{aligned} &case\ 3 : Tx \rightarrow scatterers \rightarrow reflectors \\ &case\ 4 : Tx \rightarrow reflectors \rightarrow scatterers \rightarrow reflectors. \end{aligned}$$

Signal flows of both case 1 and case 3 of matrices $\boldsymbol{sr}(f)$ and $\boldsymbol{rs}(f)$ are directly start from Tx, while the case 2 and case 4 contain the so-called reverberating effects between reflectors and scatterers.

The purpose of the following proposed embedded method is to decouple the case 2 and case 4 signal flows from matrices $\boldsymbol{sr}(f)$ and $\boldsymbol{rs}(f)$.

2) EMBEDDED METHOD

In case 2 of matrix $\boldsymbol{sr}(f)$, the scatterers at two terminals can be regarded as relay base stations. Then the sub-channel of a full propagation channel with only reflectors and scatterers can be illustrated in Fig. 5 (a), in which scatterers at two sides are transmitters and receivers, $\boldsymbol{s}(f)$ and $\boldsymbol{r}_{\mathrm{n}}(f)$ are defined in Fig. 4, $\boldsymbol{sr_1}(f)$ and $\boldsymbol{rs_1}(f)$ represent the transfer matrix from reflectors to scatterers and from scatterers to reflectors, respectively.

Then the effects of case 2 can be embedded into the the embedded-scatterers transfer matrix $\boldsymbol{ss}(f)$ as

$$\boldsymbol{ss}(f) = \boldsymbol{s}(f) + \sum_{n=2}^{\infty}\left[\boldsymbol{rs_1}(f)\boldsymbol{r}_{\mathrm{n}-1}(f)\boldsymbol{sr_{1,n}}(f)\right], \tag{26}$$

where $\boldsymbol{r}_n(f)$ represents bouncing among reflectors for n times and can be calculated by the manner of Eq. (19), $\boldsymbol{sr_{1,n}}(f)$ can be computed in the same way illustrated in Eq. (21).

In case 2 of matrix $\boldsymbol{rs}(f)$, the reflectors at two terminals illustrated in Fig. 5 (b) also can be regarded as relay base stations. Applying the same formulation in Eq. (26), the effects of case 2 can be embedded into the the embedded-reflection transfer matrix $\boldsymbol{rr}(f)$ as

$$\boldsymbol{rr}(f) = \boldsymbol{r}(f) + \sum_{n=2}^{\infty}\left[\boldsymbol{sr_2}(f)\boldsymbol{s}^{\mathrm{n}-1}(f)\boldsymbol{rs_2}(f)\right], \tag{27}$$

where $\boldsymbol{sr_2}(f)$ and $\boldsymbol{rs_2}(f)$ represent the transfer matrix from reflectors to scatterers and from scatterers to reflectors in Fig. 5 (b), respectively.

After embedded the reverberating effects of reflecting and scattering into matrices $\boldsymbol{ss}(f)$ and $\boldsymbol{rr}(f)$, we only need to consider components in case 1 of matrices $\boldsymbol{sr}(f)$ and $\boldsymbol{rs}(f)$. Then, matrix $\boldsymbol{sr}(f)$ can be calculated using the RPG approach denoted in Eq. (18), (19) and (21). The edge gains *scatterers* $\rightarrow$ *reflectors* in matrix $\boldsymbol{rs}(f)$ can be calculated using Eq. (21).

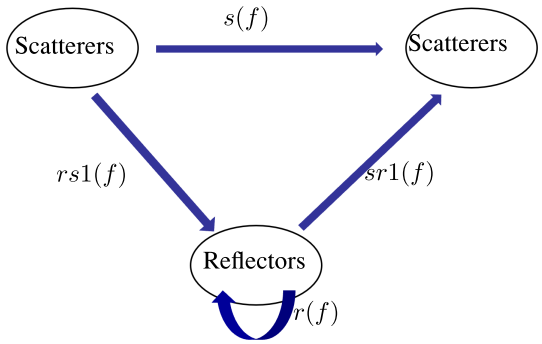

(a) Model for scattering transfer function matrix $ss(f)$

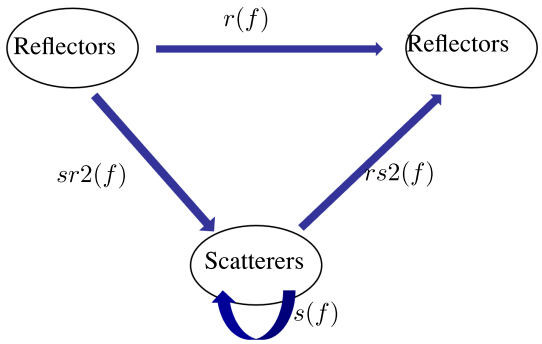

(b) Model for reflecting transfer function matrix $rr(f)$

FIGURE 5. Model for reflecting and scattering transfer function matrix.

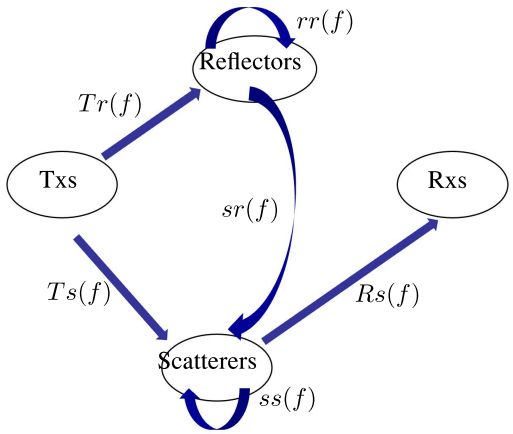

(a) Subgraph for wave received from scatterers $H_s(f)$

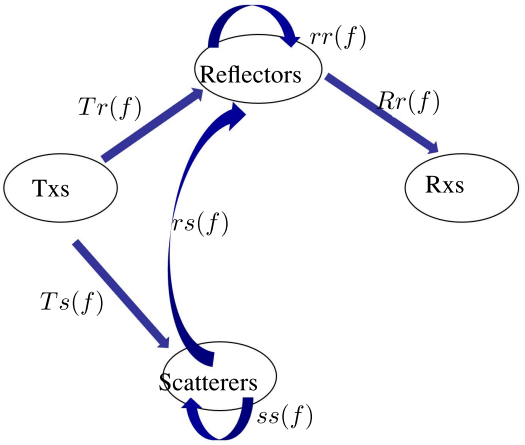

(b) Subgraph for wave received from reflectors $H_r(f)$

FIGURE 6. Subgraph for NLoS parts.

3) CALCULATION OF CHANNEL TRANSFER FUNCTION FOR EPG

The full propagation graph can be divided into three parts, i.e., the LoS parts $\boldsymbol{D}(f)$, the NLoS parts $\boldsymbol{H_s}(f)$ and $\boldsymbol{H_r}(f)$. The NLoS parts, i.e., subgraph for wave of $\boldsymbol{H_s}(f)$ and $\boldsymbol{H_r}(f)$, are illustrated in Fig. 6 (a) and (b), respectively.

The NLoS portion of channel transfer function $\boldsymbol{H_s}(f)$ can be calculated as

$$\boldsymbol{H}_s(f) = \boldsymbol{Tr}(f)\sum_{n=2}^{\infty}\Big[\boldsymbol{rr}_{\mathrm{n}-1}(f)\boldsymbol{sr}_n(f)\big[\boldsymbol{I}-\boldsymbol{ss}(f)\big]^{-1}\cdot\boldsymbol{Rs}(f)\Big] + \boldsymbol{Ts}(f)\big[\boldsymbol{I}-\boldsymbol{ss}(f)\big]^{-1}\boldsymbol{Rs}(f). \tag{28}$$

The first part denotes the propagating flows: $Tx \rightarrow$ *reflectors* $\rightarrow$ *scatterers* $\rightarrow Rx$. The second part denotes the propagating flows: $Tx \rightarrow$ *scatterers* $\rightarrow Rx$.

The NLoS portion of channel transfer function $\boldsymbol{H_r}(f)$ can be calculated as

$$\boldsymbol{H}_r(f) = \sum_{n=2}^{\infty}\Big[\boldsymbol{Ts}(f)\big[\boldsymbol{I}-\boldsymbol{ss}(f)\big]^{-1}\boldsymbol{sr}(f)\boldsymbol{r}_{\mathrm{n}-1}(f)\boldsymbol{Rr}_{\mathrm{n}}(f)\Big] + \sum_{n=2}^{\infty}\big[\boldsymbol{Tr}(f)\boldsymbol{r}_{\mathrm{n}-1}(f)\boldsymbol{Rr}_{\mathrm{n}}(f)\big]. \tag{29}$$

The first part denotes the propagating flows: $Tx \rightarrow$ *scatterers* $\rightarrow$ *reflectors* $\rightarrow Rx$. The second part denotes the propagating flows: $Tx \rightarrow$ *reflectors* $\rightarrow Rx$.

Then, the total channel transfer function can be calculated by superimposing these components as

$$\boldsymbol{H}(f) = \boldsymbol{D}(f) + \boldsymbol{H}_r(f) + \boldsymbol{H}_s(f). \tag{30}$$

After all, the $\boldsymbol{H}(f)$ includes line of sight propagation, reflecting-path, scattering-path, and reflecting-scattering mixed paths.

III. MEASUREMENT-BASED PERFORMANCE EVALUATION

A. MEASUREMENT CAMPAIGN

In this section, the EPG was evaluated by a millimeter-wave (mm-wave) field measurement in a corridor scenario. The channel sounder was constructed using a programmable network analyzer (PNA), a computer, a storage disk, oscillators, frequency doublers, amplifiers, band-pass filter and a low noise amplifier. Detailed information about the channel

TABLE 2. The parameters of measurement campaign.

Parameter	Value
Center frequency [GHz]	39
Bandwidth [GHz]	4
Number of frequency points	1001
Antenna type	Omni-directional antennas

FIGURE 7. The photo for the measurement environment of the corridor.

sounder can be found in [36], [37]. Two 39 GHz omni-antennas were used in both Tx and Rx sides. Important configuration parameters are reported in Table 2.

The measurement campaign is performed in a corridor showed in Fig. 7.

The sketch map of the corridor is depicted in Fig. 8.

The Tx was fixed at one end and the Rx was on the trolley which gradually departs forward along the route connecting Site.7 to Site.1 in the sketch map showed by Fig. 8.

B. IMPLEMENTATION PROCEDURES OF EPG

Step 1 (Set Up Digital Map According to the Geometrical Information of Environment): Divide the objects in the environment into scatterers and reflectors according to surface roughness.

In this corridor scenario, glass windows are discretized as reflecting cells, whose area dS is 0.01 m^2 with coefficient 0.2, while walls, floors, ceilings and handrails are discretized as scattering cells, whose area dS is 0.04 m^2 with coefficient 0.6. The parameters of mm-wave are justified in [15], [38] and used in unified PG in [18]. For more accurate simulation, the coefficients need to be calibrated with measurement results, even machine learning can also be applied to modify the coefficients [33].

Step 2 (Generate Transfer Matrix): Identify the scattering paths and reflecting paths of every pair of vertices, e.g., Tx and reflectors, reflectors and scatterers.

Fig. 9 and Fig. 10 illustrate one-bouncing scattering paths and one-bouncing reflection paths from Tx to Rx of one snapshot, respectively.

Then, calculate transfer matrices, i.e., $\boldsymbol{D}(f)$, $\boldsymbol{Tr}(f)$, $\boldsymbol{Ts}(f)$, $\boldsymbol{s}(f)$, $\boldsymbol{sr}(f)$, $\boldsymbol{Rs}(f)$, $\boldsymbol{r}(f)$, $\boldsymbol{rs}(f)$, $\boldsymbol{Rr}(f)$. It is reported in [18] when the bouncing order is up to 3, the influence of multi-path of mm-wave was quite weak, hence, we set $n = 4$ as the highest reflecting order in this simulation.

Step 3 (Calculate the Transfer Matrices Using EPG): Use Eq. (27) to calculate scattering-embedded transfer reflecting matrices. Use Eq. (26) to calculate reflection-embedded transfer scattering matrices. Calculate channel transfer functions by Eq. (30) and obtain the corresponding channel impulse responses (CIRs).

C. COMPARISONS AND DISCUSSION

1) CONCATENATED POWER DELAY PROFILES (CPDPS)

Fig. 11 (a), (b) and (c) illustrate the measured CPDPs, simulated CPDPs by EPG, and simulated CPDPs by conventional PG in the corridor scenario, respectively. It can be observed that the moving trajectory in delay for LoS paths are similar for both two simulations and the measurement, however, NLoS paths are different by appearance.

Some continuous NLoS paths marked as multi-path components 1 (MCP1) and MCP2 in Fig. 11 (a) and (b) can be observed both in the measurement and the EPG simulation. Delays of NLoS paths increase along with the LoS path with less power. However, for the conventional PG in Fig. 11 (c), MPC1 disappears quickly as the distance of Tx and Rx increases. Besides, obvious MPC2 track can not be observed in conventional PG.

2) POWER DELAY PROFILES (PDPS)

To elaborate the effects of the proposed EPG, the PDPs generated by conventional PG, proposed EPG and measurement are used for comparison. In both simulations of EPG and conventional PG, the variance of the noise is set to -105 dBm to emulate the thermal noise of measurement equipment.

Fig. 12 depicts comparison between measurement and conventional PG, comparison between measurement and proposed EPG, respectively in three typical snapshots. The three snapshots are marked as site.7, site.5, and site.2 in the sketch showed by Fig. 8. The LoS distance of site.7, site.5, and site.2 can be approximately calculated as 4 meters, 7.5 meters, and 15 meters, respectively.

In Fig. 12 (a), the PDPs generated by both conventional PG and the proposed EPG are able to reproduce the two NLoS peaks as the measurement when the distance of Tx and Rx is not far away.

However, as the distance between Tx and Rx increases in Fig. 12 (b), the conventional PG can only reproduce part of the NLoS peaks, while the newly proposed PG still works well, the two important NLoS peaks match the measurement with little error.

The contrast becomes more evident in Fig. 12 (c), when the distance between Tx and Rx is more than 15 meters, it can be observed that two obvious peaks for NLOS paths of EPG and measurement in around 55 ns and 57 ns coincides with each other, however, these two NLoS components are invisible in the PDP generated using the conventional PG.

3) DELAY AND DELAY SPREAD

The mean delay and delay spread of site.7, site.5, and site.2 mentioned above are listed in Table 3, from which, it is

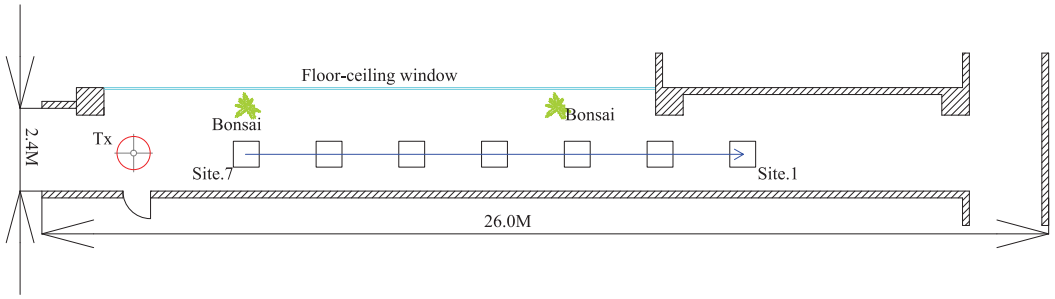

FIGURE 8. A diagram of the environment considered in the measurement, on the upper side of this sketch is glass windows, on the other side is a concrete wall.

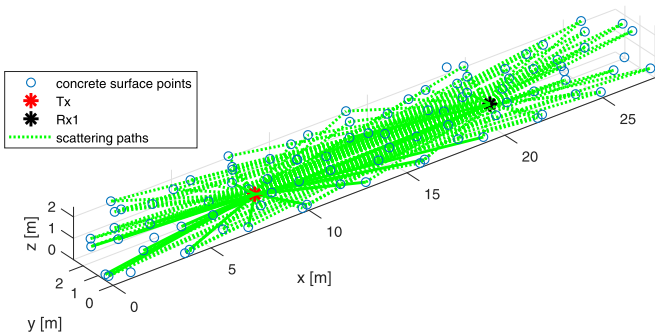

FIGURE 9. One-bouncing scattering paths illustration.

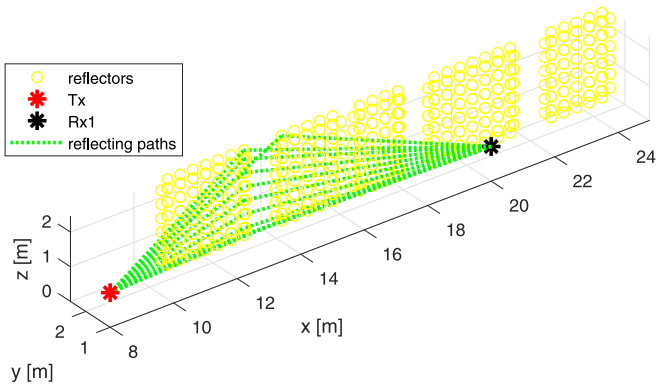

FIGURE 10. One-bouncing reflection paths illustration.

observed that delay parameters of measurement and both two simulations are in good consistency. The difference of mean delay between measurement and simulation is within 3 ns, and difference of root-mean-square is within 1.5 ns.

4) DISCUSSION OF VALIDATION

The CPDPs obtained using the newly proposed EPG provide more accurate descriptions of this time-variant channel, i.e., the reflection effects caused by the glass windows in this corridor scenario can be observed in both measurement and EPG simulation as the delay varies. Moreover, spatial consistency of the moving track is also can be inferred.

The observation of single PDP comparison is in line with CPDPs, furthermore, single PDP can explain the MPC tracks revealed in CPDPs more concretely. The scattering component becomes weaker and weaker as the distance increases, hence the MPC tracks of conventional PG fading quite fast due to lack of considering reflection effects. On the contrary, the proposed EPG always keeps consistency with measurement.

TABLE 3. The delay parameters comparison of conventional PG, EPG, and measurement.

Parameters	Conventional PG	EPG	Measurement
Mean delay of site.7 [ns]	18.66	18.66	19.11
Mean delay of site.5 [ns]	30.58	31.24	28.52
Mean delay of site.5 [ns]	54, 63	55.43	54, 72
Delay spread of site.7 [ns]	8.36	8.16	9.74
Delay spread of site.5 [ns]	7.42	7.25	7.49
Delay spread of site.2 [ns]	1.54	1.65	2.15

The mean delay and delay spread obtained through conventional PG and EPG are both in good agreement with measurement, it means the in such a corridor scenario, the LoS path plays the most vital role in propagating signals.

These observations reveal two postulations, firstly, even in the mm-wave frequency band the reflection mechanism still plays a vital role in generating multipaths. Secondly the improved EPG can simulate channels in better accordance with the measurements than the conventional PG where dominant reflection paths exist. The reasons why the simulation results are not strictly identical to the measurement, according to our conjecture, include inaccurate estimation of the Rx location, the exact radiation pattern of the omnidirectional antenna which is not considered in graph simulations, and the thermal noise in the measurement equipment, etc.

IV. CONCLUSION

In this article, a novel simulation-based channel modeling approach based on EPG is proposed and evaluated by field measurement. Distinguished from the conventional scattering PG, reflectors are added to generate a reflector-scatterer-hybrid propagation graph. Such an extended graph can imitates wave propagating along scattering-path, reflecting-path and scattering-reflecting-mixed-path. An essential specifically subgraph-embedded method is utilized, which allows decomposing mixed-path of full graph into scattering-path and reflecting-path. In addition, a recursive formulation is implemented and applied to calculating the composite effect of scattering-path and reflecting-path. The procedures of the newly proposed EPG are elaborated in this article.

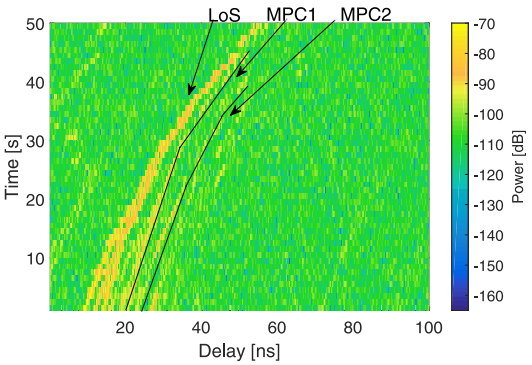

(a) CPDPs observed in measurements

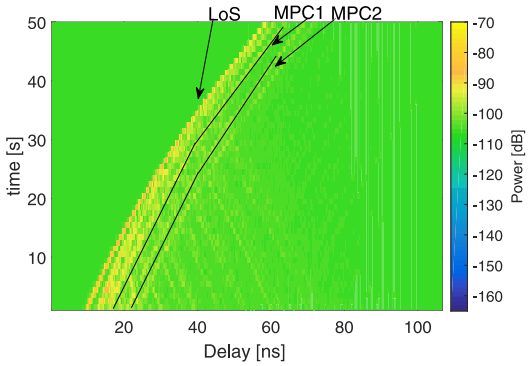

(b) CPDPs generated using EPG

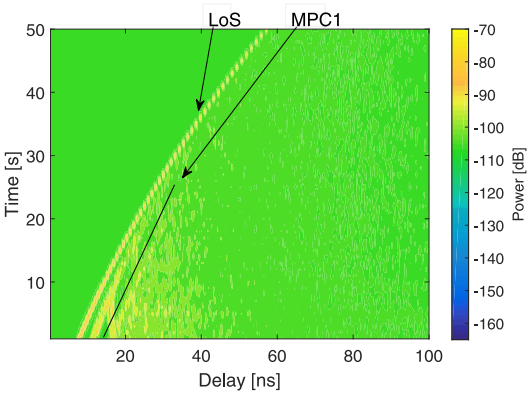

(c) CPDPs generated using PG

FIGURE 11. **CPDPs comparison for measurements, EPG simulation and conventional PG simulation.**

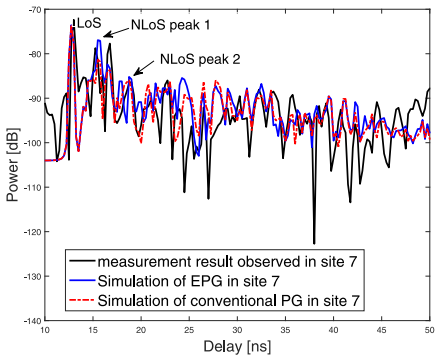

(a) PDP comparison of measurement, proposed EPG, and conventional PG in site.7

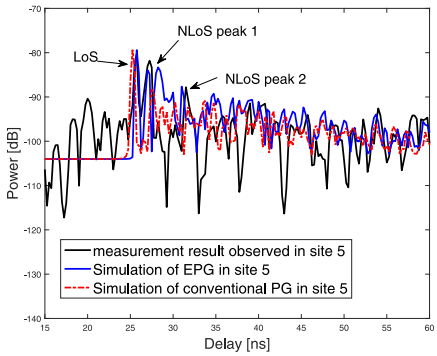

(b) PDP comparison of measurement, proposed EPG, and conventional PG in site.5

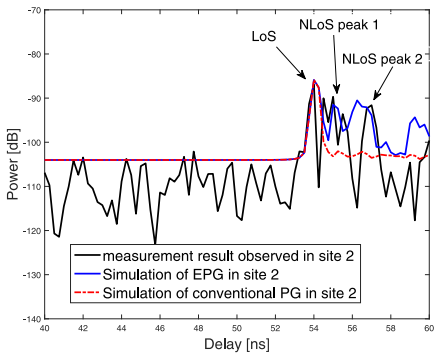

(c) PDP comparison of measurement, proposed EPG, and conventional PG in site.2

FIGURE 12. **PDPs comparison for measurements, proposed EPG, conventional PG in three typical sites.**

The comparison of CPDPs and single PDPs was performed among the conventional PG, the newly proposed EPG, and measurement in a mm-wave corridor scenario. The results demonstrate that the reflection mechanisms can not be ignored in mm-wave band frequency. With reflection effects added into the PG, the channel spatial consistency observed in NLoS scenarios was explained more reasonably in the graph simulation. With these evidences, it is concluded that the newly proposed method is capable of accordingly reproducing the channel characteristics attributed to reflecting components and scattering components.

Accurate and efficient channel simulation algorithms may provide powerful tools for wireless channel and physical layer researches, in an era of Internet of Things with increasingly frequency.

REFERENCES

[1] T. Obara, T. Okuyama, Y. Aoki, S. Suyama, J. Lee, and Y. Okumura, "Indoor and outdoor experimental trials in 28-GHz band for 5G wireless communication systems," in *Proc. IEEE 26th Annu. Int. Symp. Pers. Indoor Mobile Radio Commun. (PIMRC)*, Aug. 2015, pp. 846–850.

[2] M. S. Alouini, "Paving the way towards 5G wireless communication networks," in *Proc. 2nd Int. Conf. Telecommun. Netw. (TEL-NET)*, Aug. 2017, p. 1.

[3] Z. Cao *et al.*, "Advanced integration techniques on broadband millimeter-wave beam steering for 5G wireless networks and beyond," *IEEE J. Quantum Electron.*, vol. 52, no. 1, pp. 1–20, Jan. 2016.

[4] J. Huang, C.-X. Wang, R. Feng, J. Sun, W. Zhang, and Y. Yang, "Multi-frequency mmWave massive MIMO channel measurements and characterization for 5G wireless communication systems," *IEEE J. Sel. Areas Commun.*, vol. 35, no. 7, pp. 1591–1605, Jul. 2017.

[5] T. Abbas, J. Nuckelt, T. Kurner, T. Zemen, C. F. Mecklenbrauker, and F. Tufvesson, "Simulation and measurement-based vehicle-to-vehicle channel characterization: Accuracy and constraint analysis," *IEEE Trans. Antennas Propag.*, vol. 63, no. 7, pp. 3208–3218, Jul. 2015.

[6] C. Gustafson, K. Haneda, S. Wyne, and F. Tufvesson, "On mm-Wave multipath clustering and channel modeling," *IEEE Trans. Antennas Propag.*, vol. 62, no. 3, pp. 1445–1455, Mar. 2014.

[7] V. Degli-Esposti, D. Guiducci, A. de'Marsi, P. Azzi, and F. Fuschini, "An advanced field prediction model including diffuse scattering," *IEEE Trans. Antennas Propag.*, vol. 52, no. 7, pp. 1717–1728, Jul. 2004.

[8] A. O. Kaya, L. J. Greenstein, and W. Trappe, "Characterizing indoor wireless channels via ray tracing combined with stochastic modeling," *IEEE Trans. Wireless Commun.*, vol. 8, no. 8, pp. 4165–4175, Aug. 2009.

[9] T. Pedersen and B. H. Fleury, "A realistic radio channel model based in stochastic propagation graphs," in *Proc. 5th MATHMOD*, 2006, pp. 324–331.

[10] T. Pedersen, G. Steinbock, and B. H. Fleury, "Modeling of outdoor-to-indoor radio channels via propagation graphs," in *Proc. XXXIth URSI Gen. Assembly Sci. Symp. (URSI GASS)*, Aug. 2014, pp. 1–4.

[11] G. E. Athanasiadou, A. R. Nix, and J. P. McGeehan, "A microcellular ray-tracing propagation model and evaluation of its narrow-band and wide-band predictions," *IEEE J. Sel. Areas Commun.*, vol. 18, no. 3, pp. 322–335, Mar. 2000.

[12] B. Choudhury and R. M. Jha, "A refined ray tracing approach for wireless communications inside underground mines and metrorail tunnels," in *Proc. IEEE Appl. Electromagn. Conf. (AEMC)*, Dec. 2011, pp. 1–4.

[13] G.-Y. Wang, Y.-J. Liu, and S.-D. Li, "Simulation and analysis of indoor millimeter-wave propagation based on the ray tracing method," in *Proc. IEEE Int. Conf. Comput. Electromagn. (ICCEM)*, Feb. 2016, pp. 350–352.

[14] P. Koivumaki, S. L. H. Nguyen, K. Haneda, and G. Steinböck, "A study of polarimetric diffuse scattering at 28 GHz for a shopping center facade," in *Proc. IEEE 29th Annu. Int. Symp. Pers. Indoor Mobile Radio Commun. (PIMRC)*, Sep. 2018, pp. 182–187.

[15] E. M. Vitucci, J. Chen, V. Degli-Esposti, J. S. Lu, H. L. Bertoni, and X. Yin, "Analyzing radio scattering caused by various building elements using millimeter-wave scale model measurements and ray tracing," *IEEE Trans. Antennas Propag.*, vol. 67, no. 1, pp. 665–669, Jan. 2019.

[16] T. G. Lewis, *Graphs*. Hoboken, NJ, USA: Wiley, 2009. [Online]. Available: https://ieeexplore.ieee.org/document/8041132

[17] J. Zhang, C. Tao, L. Liu, and R. Sun, "A study on channel modeling in tunnel scenario based on propagation-graph theory," in *Proc. IEEE 83rd Veh. Technol. Conf. (VTC Spring)*, May 2016, pp. 1–5.

[18] J. Chen, X. Yin, L. Tian, and M.-D. Kim, "Millimeter-wave channel modeling based on a unified propagation graph theory," *IEEE Commun. Lett.*, vol. 21, no. 2, pp. 246–249, Feb. 2017.

[19] T. Pedersen, G. Steinbock, and B. H. Fleury, "Modeling of reverberant radio channels using propagation graphs," *IEEE Trans. Antennas Propag.*, vol. 60, no. 12, pp. 5978–5988, Dec. 2012.

[20] T. Pedersen and B. H. Fleury, "Radio channel modelling using stochastic propagation graphs," in *Proc. IEEE Int. Conf. Commun.*, Jun. 2007, pp. 2733–2738.

[21] R. Zhang, X. Lu, Z. Zhong, and C. Lin, "A study on spatial-temporal dynamics properties of indoor wireless channels," in *Proc. Wireless Algorithms Syst. Appl. Int. Conf.*, Chengdu, China, Aug. 2011, pp. 410–421.

[22] L. Tian, X. Yin, Q. Zuo, J. Zhou, Z. Zhong, and S. X. Lu, "Channel modeling based on random propagation graphs for high speed railway scenarios," in *Proc. IEEE 23rd Int. Symp. Pers. Indoor Mobile Radio Commun. (PIMRC)*, Sep. 2012, pp. 1746–1750.

[23] Y. Miao, T. Pedersen, M. Gan, E. Vinogradov, and C. Oestges, "Reverberant room-to-room radio channel prediction by using rays and graphs," *IEEE Trans. Antennas Propag.*, vol. 67, no. 1, pp. 484–494, Jan. 2019.

[24] R. Adeogun, A. Bharti, and T. Pedersen, "An iterative transfer matrix computation method for propagation graphs in multiroom environments," *IEEE Antennas Wireless Propag. Lett.*, vol. 18, no. 4, pp. 616–620, Apr. 2019.

[25] O. Souihli and T. Ohtsuki, "Benefits of rich scattering in MIMO channels: A graph-theoretical perspective," *IEEE Commun. Lett.*, vol. 17, no. 1, pp. 23–26, Jan. 2013.

[26] Y. Liu, X. Yin, J. Lee, and M. Tong, "A graph-based simulation method for propagation channels with multiple-knife-edge diffraction," in *Proc. IEEE Int. Conf. Comput. Electromagn. (ICCEM)*, 2020, pp. 270–272.

[27] A. F. Molisch, *Propagation Mechanisms*. Hoboken, NJ, USA: Wiley-IEEE Press, 2011. [Online]. Available: https://ieeexplore.ieee.org/document/5635436

[28] X. Yin and X. Cheng, "Propagation channel characterization, parameter estimation, and modeling for wireless communications," in *Deterministic Channel-Parameter Estimation*. Hoboken, NJ, USA: Wiley-IEEE Press, 2016. [Online]. Available: https://ieeexplore.ieee.org/document/7656797

[29] T. K. Sarkar, M. Salazar Palma, and M. N. Abdallah, *Mechanism of Wireless Propagation*. Hoboken, NJ, USA: Wiley-IEEE Press, 2018. [Online]. Available: https://ieeexplore.ieee.org/document/8410155

[30] L. Tian, V. Degli-Esposti, E. M. Vitucci, and X. Yin, "Semi-deterministic radio channel modeling based on graph theory and ray-tracing," *IEEE Trans. Antennas Propag.*, vol. 64, no. 6, pp. 2475–2486, Jun. 2016.

[31] L. Tian, V. Degli-Esposti, E. M. Vitucci, X. Yin, F. Mani, and S. X. Lu, "Semi-deterministic modeling of diffuse scattering component based on propagation graph theory," in *Proc. IEEE 25th Annu. Int. Symp. Pers. Indoor Mobile Radio Commun. (PIMRC)*, Sep. 2014, pp. 155–160.

[32] G. Steinböck *et al.*, "Hybrid model for reverberant indoor radio channels using rays and graphs," *IEEE Trans. Antennas Propag.*, vol. 64, no. 9, pp. 4036–4048, Sep. 2016.

[33] R. O. Adeogun, "Calibration of stochastic radio propagation models using machine learning," *IEEE Antennas Wireless Propag. Lett.*, vol. 18, no. 12, pp. 2538–2542, Dec. 2019.

[34] A. Goldsmith, *Wireless Communications, Path Loss and Shadowing*. Cambridge, U.K.: Cambridge Univ. Press, 2005, pp. 27–63.

[35] D. M. Pozar, *Microwave Engineering—Transmission Line Theory*, 4th ed. New Delhi, India: Wiley, 2012, pp. 68–114.

[36] Y. Lv, X. Yin, C. Zhang, and H. Wang, "Measurement-based characterization of 39 GHz millimeter-wave dual-polarized channel under foliage loss impact," *IEEE Access*, vol. 7, pp. 151558–151568, 2019.

[37] C. Zhang, X. Yin, X. Cai, and Z. Yu, "Wideband 39 GHz millimeter-wave channel measurements under diversified vegetation," in *Proc. IEEE 29th Annu. Int. Symp. Pers. Indoor Mobile Radio Commun. (PIMRC)*, Sep. 2018, pp. 1–6.

[38] V. Degli-Esposti *et al.*, "Ray-tracing-based mm-Wave beamforming assessment," *IEEE Access*, vol. 2, pp. 1314–1325, 2014.

YUAN LIU received the bachelor's degree in electronics engineering from Central China Normal University, Wuhan, China, in 2017, and the master's degree in electronics engineering from Tongji University, Shanghai, China, in 2020. From September 2018 to June 2019, he was a Visitor with the Group of Antennas and Propagation, Aalto University, Helsinki, Finland. He is currently a Research Engineer with Guangdong Communications & Networks Institute. His research interests include radio propagation simulation tools, such as propagation-graph and ray-tracing, statistical signal processing for channel parameters estimation and characterization, terahertz channel modeling and terahertz/RF systems for B5G communications.

XUEFENG YIN (Member, IEEE) received the bachelor's degree in optoelectronics engineering from the Huazhong University of Science and Technology, Wuhan, China, in 1995, and the M.Sc. degree in digital communications and the Ph.D. degree in wireless communications from Aalborg University, Aalborg, Denmark, in 2002 and 2006, respectively. From 2006 to 2008, he was an Assistant Professor with Aalborg University. In 2008, he joined the College of Electronics and Information Engineering, Tongji University, Shanghai, China. He became a Full Professor, in 2016, and has been the Vice Dean of the College of Electronics and Information Engineering since then. He has authored or coauthored more than 100 technical articles and coauthored the book *Propagation Channel Characterization, Parameter Estimation, and Modeling for Wireless Communications* (Wiley, 2016). His research interests include high-resolution parameter estimation for propagation channels, measurement-based channel characterization and stochastic modeling for 5G wireless communications, channel simulation based on random graph models, radar signal processing, and target recognition.

XIAOKANG YE (Student Member, IEEE) received the bachelor's degree in electrical engineering from the Shanghai University of Engineering Science, Shanghai, China, in 2014. He is currently pursuing the Ph.D. degree with the College of Electronics and Information Engineering, Tongji University. His research interests include statistical channel characterization, millimeter wave channel characterization and modeling, channel fingerprint, and applications of machine learning based techniques on propagation channel characterization.

YONGYU HE (Student Member, IEEE) was born in Pingan, China, in 1989. He received the bachelor's degree in electronics science and technology and the master's degree in circuit and systems from the Tongji University, Shanghai, China, in July 2011 and April 2014, respectively, where he is currently pursuing the Doctoral degree in physics. His research interests include wireless propagation channel and more specifically, the characterization and modeling of millimeter-wave and higher frequency band channels, and self-interference channels.

JUYUL LEE (Senior Member, IEEE) received the Ph.D. degree in electrical engineering from the University of Minnesota at Twin Cities, USA, in 2010. He was with the Agency for Defense Development, Daejeon, South Korea, from 1998 to 2000. Since 2000, he has been with the Electronics and Telecommunications Research Institute, Daejeon, where he is currently a Principal Researcher with the Telecommunications and Media Research Laboratory. He has contributed to ITU-R recommendations and reports in Study Group 3 (Propagation), including millimeter-wave propagation models. He is currently the Chairman of the ITU-R Correspondence Group 3K-6, which is responsible for studying the impact of higher frequencies (from 6 GHz to 450 GHz) on propagation models and related characteristics. His current research interests include wireless channel modeling, machine learning, and information theory.